Title

A STUDY OF THE APPLICATION OF MERCURY POROSIMETRY METHOD TO A SINGLE FRACTURE

Authors

Tsang, Y.W.
Hale, F.V.

Publication Date

1988-06-01

Lawrence Berkeley Laboratory
UNIVERSITY OF CALIFORNIA

EARTH SCIENCES DIVISION

To be published in the Proceedings of the
International Conference on Fluid Flow in
Fractured Rocks, Atlanta, GA, May 15–17, 1988

A Study of the Application of Mercury Porosimetry Method to a Single Fracture

Y.W. Tsang and F.V. Hale

June 1988

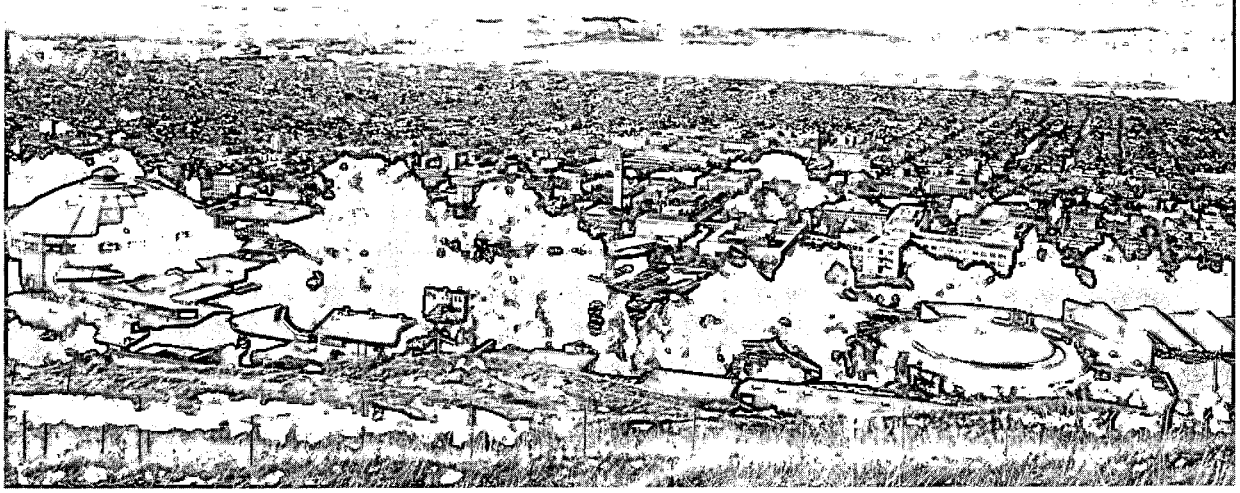

Prepared for the U.S. Department of Energy under Contract Number DE-AC03-76SF00098.

DISCLAIMER

A Study of the Application of Mercury Porosimetry Method to a Single Fracture

Y. W. Tsang and F. V. Hale

Earth Sciences Division
Lawrence Berkeley Laboratory
University of California
Berkeley, California 94720

ABSTRACT

In recent years, there is increasing evidence both in the field and in the laboratory that the fluid flow in low permeability fractured media is unevenly distributed and predominantly occurs in selected preferred paths. In view of the experimental observation of flow channeling, conceptual models (Tsang and Tsang, 1987; Tsang et al., this volume 1988b) have been developed to interpret fluid flow and transport in fractured media as through a system of statistically equivalent channels, and to relate permeability and tracer transport measurements to fracture aperture parameters.

Mercury porosimetry has long been used to study the void space of porous materials. In this paper, we apply the concept of mercury porosimetry for porous rock to a rock fracture by simulations of mercury intrusion and withdrawal in a single fracture with variable apertures. Our theoretical studies show that the total capillary pressure curve in a pressure-controlled test gives information on the distribution of all the apertures which control the tracer transport through the fracture. On the other hand, the second intrusion curve in a pressure-controlled experiment resembles the rison part of a rate-controlled experiment (Yuan and Swanson, 1986), and gives information on the small aperture distribution which control the flow permeability of the fracture. The ratio of the limiting mercury volumes of the second intrusion and the first intrusion capillary curves can confirm estimates of equivalent apertures derived from permeability and tracer transport measurements. Lastly, the fraction of trapped mercury may be related to the spatial correlation of the aperture variation in the fracture.

Introduction

Mercury porosimetry, or the measurement of capillary pressure as a function of intruded mercury volume has long been used to characterize the void spaces of porous materials. Since the introduction of the technique to the petroleum industry by Purcell (1949), mercury porosimetry has become a standard test on reservoir core samples to aid in the estimation of residual oil saturation (Pickell et al., 1966), the determination of the pore structure of the reservoir rocks (Wardlaw and Taylor, 1976), and the calculation of permeability (Swanson, 1981; Thomeer, 1983).

In this paper we apply the concept of mercury porosimetry for porous rock to a rock fracture. We investigate how capillary pressure measurements can give information on the fracture apertures, which we believe control the fluid flow and tracer transport in fractures (Tsang et al., 1988b). In the literature, rock fractures have commonly been conceptualized as a pair of smooth parallel plates. These parallel-plate fractures, each characterized by a constant aperture, serve as the basis for most models of flow and transport in a fractured media. However, in recent years, there is increasing experimental evidence both in the laboratory and in the field that the majority of flow in a rock fracture does not occur in the entire plane of the fracture, as the parallel-plate idealization of a rock fracture would predict, but tends to concentrate in preferred tortuous pathways, or channels. The field experiment in a single granitic fracture (Bourke, 1987) is a clear example of the "channeling" phenomenon. Five parallel boreholes were drilled in the plane of the single fracture two meter in extent in the wall of a quarry in Cornwall. The boreholes were packed off in contiguous 8 cm sections. Each borehole was pressurized in turn, and the fluid flow rate into the adjacent borehole is measured in cross-hole packer tests. The flow rates between the packed off sections are shown in Figure 1. That the flow takes place in channels occupying only 10 to 20% of the fracture surface is clear. We demonstrated by theoretical studies (Tsang et al., 1988b), that heterogeneities from a broad spectrum of apertures in the fracture plane alone can give rise to flow channeling. In that study, the fracture was mathematically characterized by an aperture density distribution and a spatial correlation length. It was shown that the tracer transport measurements can be expressed in terms of the aperture parameters which characterize the fracture. In the present study, we explore the possibility of mercury porosimetry measurements to delineate the fracture aperture parameters which control the fluid and mass transport.

Rate-controlled versus pressure-controlled mercury porosimetry

A fracture having a wide range of apertures may be simulated using geostatistical methods (Tsang et al., 1988a; and Moreno et al., 1988). Figure 2 shows two examples of simulated fractures with variable apertures. The sizes of the apertures are represented by the shading in the figure, the darker the shading, the smaller the aperture. Both fractures are characterized by the lognormal aperture density distribution:

$$n(b) = \frac{1}{\sqrt{2\pi}\,(\ln 10\,\sigma)^2\, b}\, \exp\left(-\frac{(\log b - \log b_o)^2}{2\sigma^2}\right) \qquad (1)$$

with the same parameters $\log b_o = 1.7$ and $\sigma = 0.43$ where the apertures are in in units of microns (μ). Figures 2a and 2b differ only in the spatial correlation length, λ: Figure 2a is generated with $\lambda/L = 0.1$ and Figure 2b with $\lambda/L = 0.4$, where L is the linear dimension of the fracture. Because mercury is a non-wetting fluid, for mercury intrusion experiment, applied pressure is needed to overcome the capillary pressure, P_c. For a fracture with spatially varying aperture, the local capillary pressure is given by:

$$P_c \approx \frac{-\sigma \cos\theta}{b} \qquad (2)$$

where σ is the interfacial tension, θ is the contact angle, and b is the local aperture. As P_c is inversely proportional to the local aperture, it is clear that the large apertures will be filled first, then smaller apertures will be filled progressively by the intruding mercury as injection pressure is increased. Mercury porosimetry experiments are usually carried out by stepping the injection pressure in small increments. At each pressure, the system is allowed to come to equilibrium before the volume of intruded mercury is recorded. The measurements are then plotted as the capillary pressure versus volume of intruded mercury, as shown schematically in Figure 3a. This kind of measurement procedure may be defined as a pressure-controlled experiment.

Yuan and Swanson (1986) proposed an experimental technique where the volumetric rate of mercury injection is kept constant and the mercury pressure is monitored. Yuan and Swanson defined their experimental method as rate-controlled porosimetry. By monitoring the capillary pressure in a rate-controlled mercury intrusion experiment, additional information regarding the pore space of a rock sample can be obtained. This will be demonstrated with the schematic diagram in Figure 3b. The work of Yuan and Swanson (1986) is on porous rock, but the following discussion will be worded in terms of mercury porosimetry applied to a rock fracture, the subject

matter of the present paper. In the rate-controlled experiment illustrated in Figure 3b, intruded mercury volume is proportional to time. Thus, one moves along the horizontal axis at a constant rate while monitoring the pressure on the vertical axis. From *a* to *b*, the pressure increases as progressively smaller apertures in the fracture are being filled. The capillary pressure at *b* corresponds to an aperture constriction which has just been filled and which acts as a barrier in the intrusion experiment. That is, the spatial distribution of the fracture apertures is such that there exist as yet unfilled pore spaces, with apertures apertures which are connected and larger than the just filled aperture constriction. These large aperture pores became accessible as the constriction is being intruded. In this case, if the rate of mercury injection is kept constant, mercury will begin to move out of the filled smaller apertures into the yet unfilled larger apertures; hence the pressure drops rapidly with negligible change of intruded mercury volume. Pressure climbs again from *c* as mercury intrudes into progressively smaller apertures until at *d*, the pressure has reached the original value at *b* before the sharp pressure drop. The pressure rises at *d* since all apertures contiguous to the filled ones now have smaller apertures. The portion of curve *bcd* will not be seen in the pressure-controlled experiment shown in Figure 3a, instead the capillary pressure curve will go from *b* to *d* horizontally, indicated by the dotted line in Figure 3b. The horizontal section *bd* arises because the prevailing pressure at *b* corresponds to the capillary pressure of the aperture constriction, so that all the apertures that are larger than the constriction, and are contiguous to the filled apertures, will be filled, moving the volume out to *d* with no change of pressure. The total capillary curve obtained from the conventional pressure-controlled mercury porosimetry will follow *abdeijp* in Figure 3b; whereas the rate-controlled mercury porosimetry shall give the additional information on the larger apertures behind small aperture constrictions as contained in the portion of curves *bcd*, *efghi*, *jklmnop*.

Yuan and Swanson (1986) defined those portions of curve which give new information of the large pore systems behind pore throats (terminology specific to porous rocks) the subison pore systems. The part of the capillary curve with the subison volumes removed is defined by Yuan and Swanson as the rison curve. The rison curve therefore is a composite of the segments *ab*, *de*, *ij*, and so on, with the segment *de* translated in the -x direction until *d* coincides with *b*, and the segment *ij* translated until *i* coincides with *e*. The rison curve is distinct from the total capillary curve shown in Figure 3a in that the asymptotic mercury volume reached here is only a

fraction of that in the total capillary curve. This is because the rison curve encompasses only the set of apertures within the two-dimensional fracture which constituted the "connected backbone" of the continuous flow paths. This subset of fracture apertures includes all the aperture constrictions and excludes the larger apertures behind the small aperture barriers. Since the local resistance to fluid flow is inversely proportional to the cube of the local aperture, this subset of apertures in the rison curve would play the dominant role in flow permeability measurements. The large apertures in the total capillary curve that are excluded in the rison capillary curve are not expected to contribute much additional resistance to the flow, they therefore play little role in permeability measurements. On the other hand, in a tracer experiment, the mean arrival time will be affected by all the apertures in the fracture, and perhaps more significantly by the larger apertures, those same ones which are excluded from the rison curve. So all the apertures in the total capillary curve participate in determining mean tracer residence time in the fracture, but only the apertures in the rison curve play a crucial role in determining the permeability of the fracture.

It will be seen that both the total capillary curve resulting from the pressure-controlled mercury porosimetry, and the rison curve resulting from rate-controlled mercury porosimetry may be simulated for a rock fracture. We shall study the simulated results with a view to interpret mercury porosimetry data in order to give pertinent flow and transport parameters.

Simulation of mercury intrusion and withdrawal experiments

We begin our calculations with the generation of variable apertures in a single fracture as shown in Figure 2. We consider a geometry where the fracture is first evacuated, and mercury is intruded simultaneously along all four edges of the fracture. At each pressure, P_c , the volume of mercury needed to fill those apertures that have a continuous mercury connection to the four edges, and are larger than the apertures associated with the prevailing capillary pressure according to Equation 1 is calculated. We assume a constant contact angle of $\theta=180^o$. This gives rise to the total capillary curve. Since all the aperture values and their spatial variation in the fracture is known, in the simulations we can also identify (1) those small aperture constrictions which define the entry pressure to a subison system of larger apertures (i.e., the pressures b, e, j in Figure 3b), and (2) the volume of the subison system of large apertures behind each aperture barrier. The above information allows us to simulate the rison

capillary curve. Figure 4 shows an example of such a simulation for the fracture shown in Figure 2a. On the x axis is plotted the filled volume of mercury in the fracture, V_f, normalized to V_t, which is the total available volume of apertures in the fracture. On the y axis, the pressure is expressed in units of 1/b (μ^{-1}), based on the implicit assumption that the interfacial tension, σ and the contact angle θ remain constant throughout the experiment. As we have pointed out earlier, the asymptotic mercury volume reached in the rison capillary curve is only a fraction of that reached in the total capillary curve; in this example, the fraction is about one third.

Since the volume of a fracture is directly proportional to the fracture aperture, b, the limiting volumes reached in the capillary curves are essentially measures of some mean aperture. So the limiting volume reached in the rison curve corresponds to some measure of a mean aperture of the subset of constrictive apertures which form the connected backbone of continuous flow paths in the fracture. On the other hand, the limiting volume reached in the total capillary curve corresponds to the mean aperture of all the apertures in the fracture. Based on our earlier discussions, one would then expect that the former mean aperture should relate to that deduced from a permeability measurement, and the latter mean aperture should relate to the mean aperture deduced from the mean residence time from a tracer transport measurement. In other words, if the permeabilty and tracer measurements through a single fracture are analyzed as if the flow and transport take place between a pair of parallel plates, then the mean separation of the parallel plates deduced from permeability measurements should be smaller that that deduced from the tracer measurements. In our simulated example, the ratio is approximately one-third. That the parallel-plate equivalent aperture derived from permeability test is smaller than that derived from tracer residence time data has been observed in the field (Abelin et al., 1985) for granitic single fractures of 5 to 10m in extent. On the laboratory scale, Gale (1987; this volume 1988) has measured the mean aperture derived from fluid flow test on two 15 cm granitic cores, each containing a single natural fracture. After the flow tests, the single fractures were injected with a room temperature curing resin. The fracture was sectioned and the trace of the resin is digitized to provide a direct measure of the distribution of all the fracture apertures. Gale (1988) found that the mean aperture derived from the resin-impregnation technique was a factor of three to ten times larger than that derived from the fluid flow test.

From the above discussions, we see that mercury porosimetry can give information on the parameters that control fluid flow and tracer transport as follows:

$$\frac{(V_f/V_t)_{rison}}{(V_f/V_t)_{total}} \approx \frac{(\bar{b})_{permeability}}{(\bar{b})_{tracer}} \tag{3}$$

On Figure 4 we also display the simulated mercury withdrawal curve from the fracture. As the mercury injection pressure is being released, the non-wetting mercury in those fracture segments with apertures that are smaller than $|-\sigma\cos\theta/P_c|$ where P_c is the current capillary pressure, will spontaneously flow out of the fracture if there exists a continuous path of mercury to the four edges. Since the mercury would stay in place where the apertures are larger then $\sigma\cos\theta/P_c$, breakage of the continuous mercury phase occur during mercury retraction. This phenomenon of breakage or "snap-off" is still not well-understood. As mercury is being expelled from the fracture with the release of external pressure, the smallest apertures will empty first, and mercury in large apertures may become isolated and trapped. Figure 4 shows that, for the example shown, about 65 % of the total volume of mercury is trapped in the fracture when the external pressure is reduced to zero. Since the mercury in the smaller apertures that formed a continuous path will be expelled in the withdrawal experiment, one may expect the withdrawal curve to have very similar shape as the rison curve of the rate controlled test. In Figure 5 the mercury withdrawal curve is shifted toward the left to the origin and compared with the rison curve. The curve is labeled withdrawal or second intrusion since a simulated second intrusion curve will be identical to the translated withdrawal curve (based on the assumption that the hysteresis due to different advancing and retracting contact angles is negligible). Figure 5 therefore illustrates that the second intrusion curve in a conventional pressure-controlled experiment may be a good approximation of the rison part of the intrusion curve obtainable in a rate-controlled experiment. While the first intrusion curve provides information on the apertures in the fracture which control the tracer transport, the second intrusion curve provides information on the aperture constrictions which control the permeability through the fracture.

Figure 6 shows the time sequence of mercury intrusion into the fracture with aperture variation shown in Figure 2a. Each snapshot in the sequence is labeled with the fraction of filled mercury volume V_f/V_t and fraction of filled fracture area, a/a_t. The hatched region represents mercury filled apertures, the blank region represents

unfilled apertures. The blank areas in the last snapshot of the sequence correspond to areas of zero apertures as we have started with a fracture that has about 13% contact area. Figure 7 shows the time sequence of mercury withdrawal. The black areas correspond to areas of zero apertures, and the white areas have been emptied. We note that in the first snapshot with slight release of the mercury injection pressure, those apertures that are emptied of mercury are the small apertures that are closest to the contact areas. In snapshot four, with mercury injection pressure equal to zero, we note that the isolated patches of large apertures with trapped mercury occupy a fractional area of about 25% of the fracture surface, which corresponds to about 65% of the total aperture volume in the fracture.

Since the residual trapped mercury is predominantly in the large apertures that are isolated by the continuous backbone of small apertures, one may expect that the smaller the spatial correlation length of the aperture variation in the fracture, the more opportunity there is for the occurrence of these isolated patches of large apertures. Figure 2 seems to support the above hypothesis. One may expect from examining Figure 2 that a greater volume of mercury will be trapped in a fracture with spatial correlation $\lambda/L=0.1$ than one with $\lambda/L=0.4$. Figure 8 shows the actual simulation of the total intrusion and withdrawal curves for both fractures of Figure 2. Indeed, the simulation shows that the trapped volume of mercury for the fracture in Figure 2b is 30% of the total fracture volume, as compared to about 56% for the fracture in Figure 2a. The simulations were done for open fractures with zero contact area. Results of a more systematic study are shown in Figure 9 where the residual mercury volume is plotted against the spatial correlation of the aperture variation. Each point corresponds to a simulated result from a different statistical realization of the same fracture aperture distribution. It is apparent from the figure that the amount of trapped mercury decreases as the spatial correlation length increases. Figure 9 demonstrates that a measurement of residual mercury volume in a mercury withdrawal experiment may give useful information on the spatial correlation length of the aperture variation. The spatial correlation length of the aperture variation has been shown to be related to the spatial distribution of flow channeling phenomena in fractures (Tsang et al., 1988a; 1988b).

Summary

We have studied the utility of applying the well known technique of mercury porosimetry to rock fractures by simulations of mercury intrusion and withdrawal in a single fracture with variable apertures. Our theoretical studies show that the total capillary pressure curve in a pressure-controlled test gives information on the distribution of all the apertures which controls the tracer transport times through the fracture. On the other hand, the second intrusion curve in a pressure-controlled experiment resembles the rison part of a rate-controlled experiment and gives information on the distribution of small apertures which controls the flow permeability of the fracture. The ratio of the limiting mercury volumes of the second intrusion and the first intrusion capillary curves can provide estimates of equivalent apertures derived from permeability and tracer transport measurements (Equation 3). Lastly, the fraction of trapped mercury may be related to the spatial correlation of the aperture variation, being larger for fractures with smaller spatial correlation length.

Acknowledgments

We gratefully acknowledge C. F. Tsang and K. Pruess of Lawrence Berkeley Laboratory for helpful discussions and review of the manuscript. The work was supported in part by the assistant secretary for Energy Research, Office of Basic Energy Sciences, Division of Engineering and Geosciences, and by the Office of Civilian Radioactive Waste Management, Office of Geologic Repositories, Engineering and Geotechnology Division, through U. S. Department of Energy contract DE-AC03-96SF00098

Selected References

Abelin, H., Neretnieks, I., Tunbrant, S., Moreno, L., 1985, Final report of the migration in a single fracture, experimental results and evaluations: Stripa Project, Sven Kärbränslefösorjning Tech. Rep. 85-03, Nucl. Fuel Safety Proj., Stockholm, Sweden.

Bourke, P.J., 1987, Channeling of flow through fractures in rock: Proc. of GEOVAL-87 International Symposium, Stockholm, Sweden, April 7-9.

Gale, J.E., 1987, Comparison of coupled fracture deformation and fluid flow models with direct measurements of fracture pore structure and stress-flow properties: Proc. 28th U.S. Symp. of Rock Mechanics, Tuscon, AZ, June 29- July 1, p. 1213-1222.

Gale, J.E., 1988, Characterizing the geometry of fracture systems for flow and transport studies in fractured rock masses: Proc., International Conference on fluid flow in fractured rocks, Atlanta, Georgia, May 15-18, p.

Moreno, L., Tsang, Y.W., Tsang, C.F., Hale, F.V. and Neretnieks, I., 1988, Flow and tracer transport in a single fracture-- a stochastic model and its relation to some field observations: in print, Water Resour. Res.

Purcell, W.R., 1949, Capillary pressure--their measurement using mercury and the calculation of permeability therefrom: Trans. AIME, v.186, p. 39-48.

Pickell, I.J., Swanson, B.F. and Hickman, W.B., 1966, Application of air-mercury and oil-water capillary pressure data in the study of pore structure and fluid distribution: Soc. Pet. Eng. J., v.18, p. 55-61

Swanson, B. F., 1981, A simple correlation between permeabilities and mercury capillary pressures: J. Pet. Tech., v.33, p. 2498-2504.

Thomeer, J.H.M., 1983, Air permeability as a function of three pore network parameter: J. Pet. Tech., v.35, p. 809-814.

Tsang, Y.W., Tsang, C.F., 1987, Channel model of flow through fractured media: Water Resour. Res. v.23(3), p. 467-479.

Tsang, Y.W., Tsang, C.F., Neretnieks, I. and Moreno, L., 1988a, Flow and tracer transport in fractured media-- variable-aperture channel model and its properties: in print, Water Resour. Res.

Tsang, C.F., Tsang, Y., and Hale, F.V., 1988b, Tracer transport in fractured rocks: Proc., International Conference on Fluid Flow in Fractured Rocks, Atlanta, GA, U.S.A., May 15-18, p.

Wardlaw, N.C. and Taylor, R.P., 1976, Mercury capillary pressure curves and the interpretation of pore structure and capillary behavior in reservoir rocks: Bull. Canadian Pet. Geol., v.24(2), p. 225-262.

Yuan, H.H., and Swanson, B.F., 1986, Resolving pore space characteristics by rate-controlled porosimetry: Soc. Pet. Eng., paper 14892 presented at the SPE/DOE Fifth Symposium on Enhanced Oil Recovery, Tulsa, OK., April 20-23.

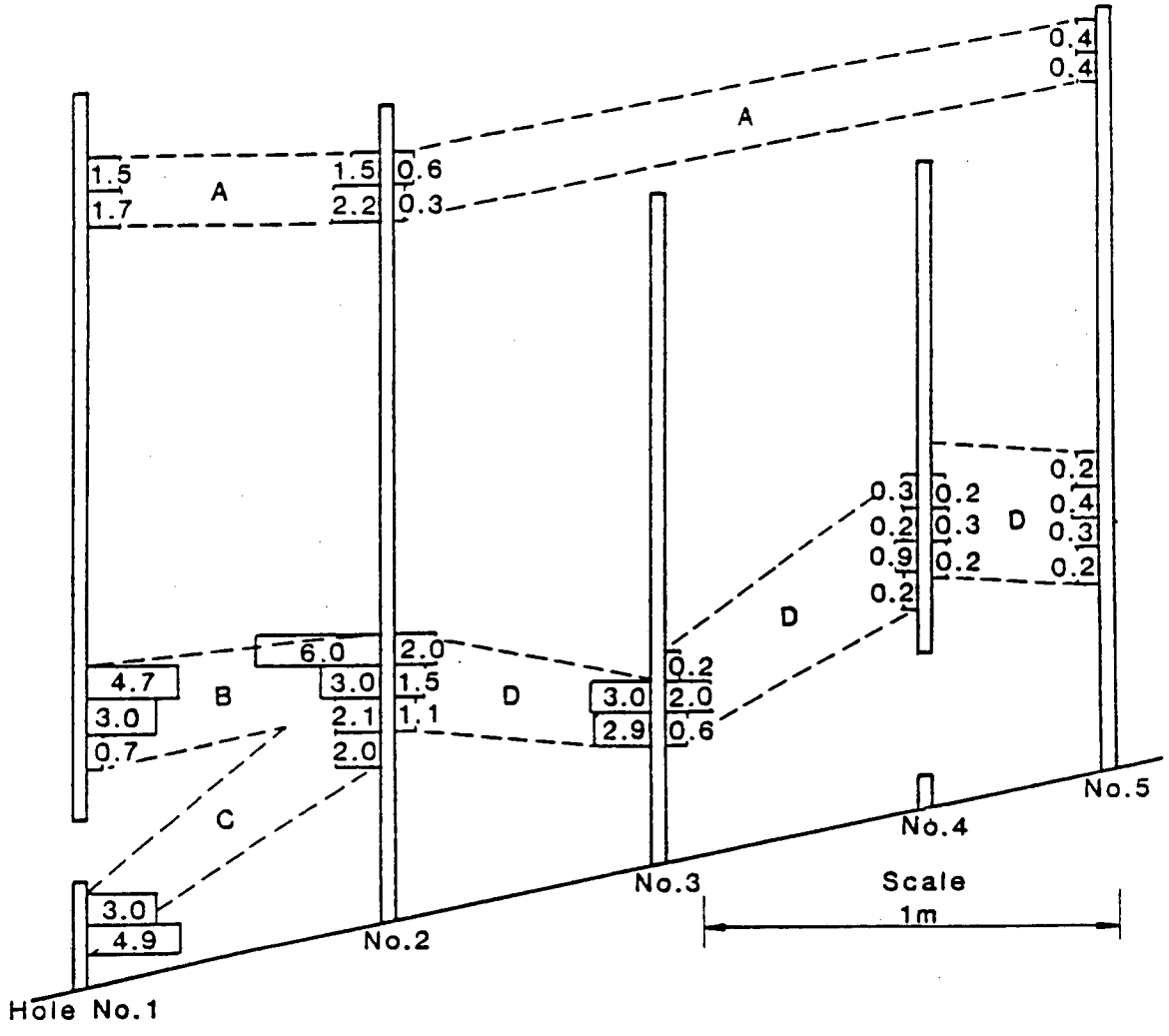

Numbers on histograms are flows in ml/sec from adjacent holes

XBL 878-3418

Figure 1. Plan view of fracture with flows into five boreholes and suggested flow channels (Bourke, 1987)

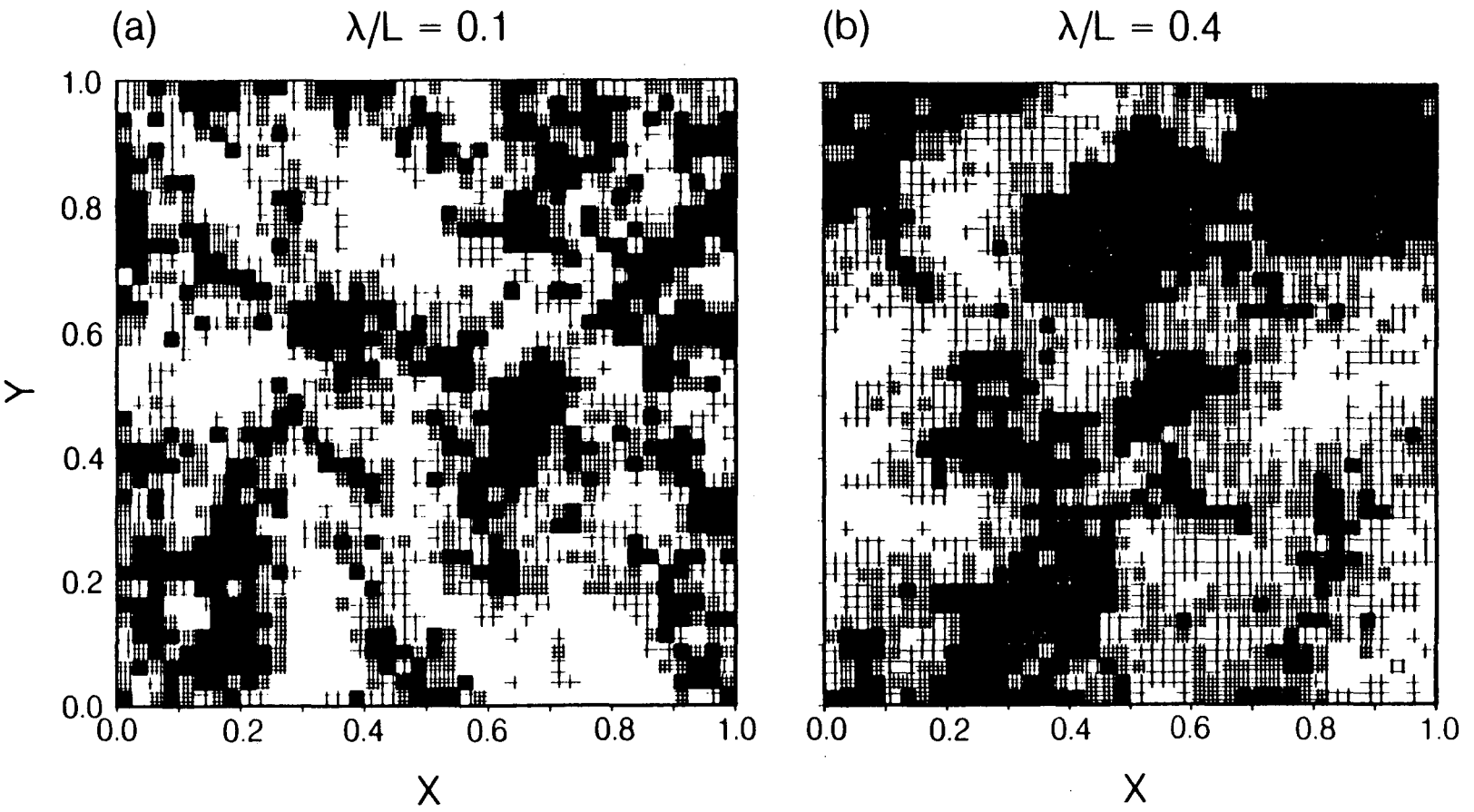

Figure 2. Statistically generated apertures with the same lognormal aperture density distribution but with different spatial correlation length, λ.

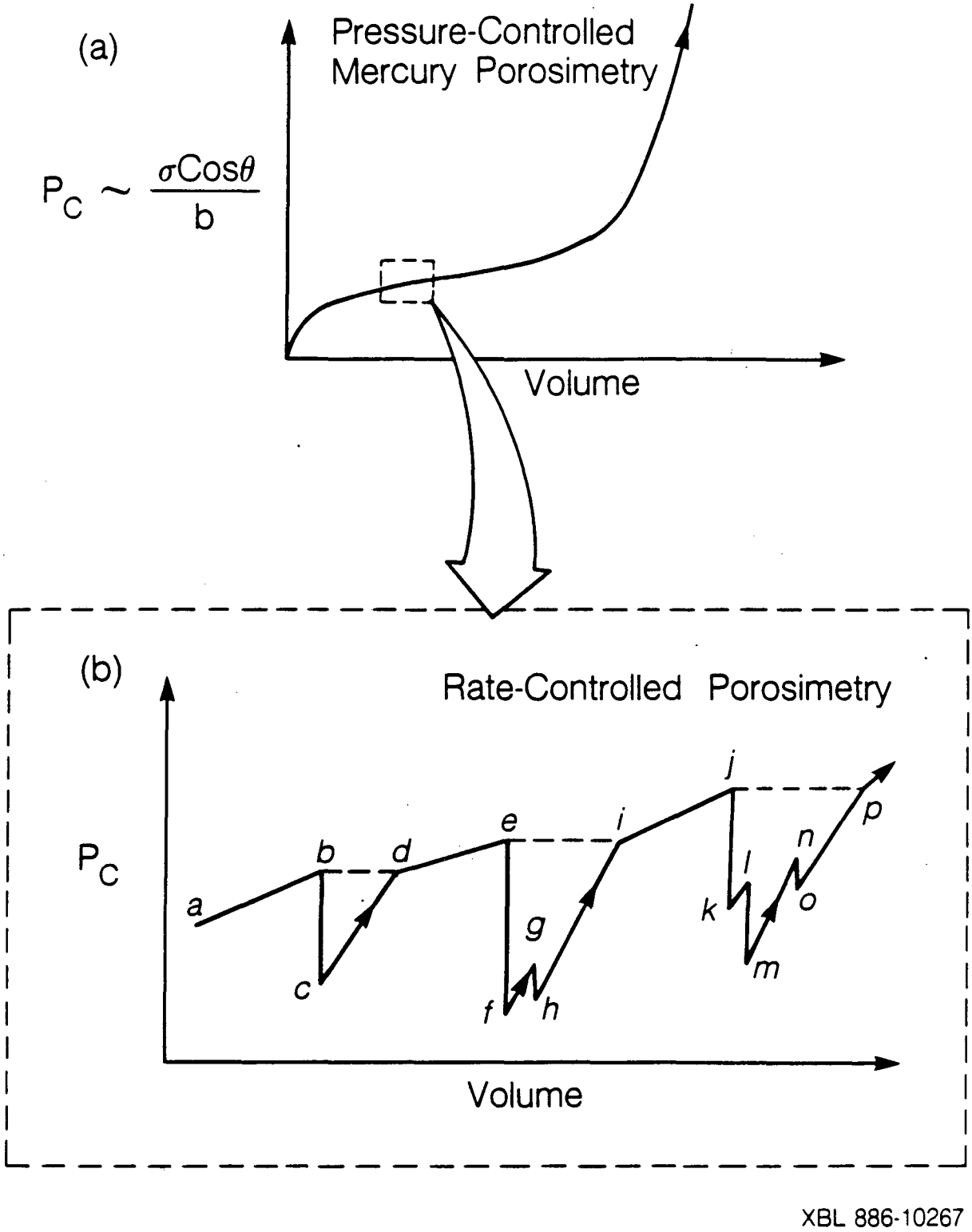

Figure 3. Schematic diagrams of capillary pressure curves from mercury porosimetry measurements.

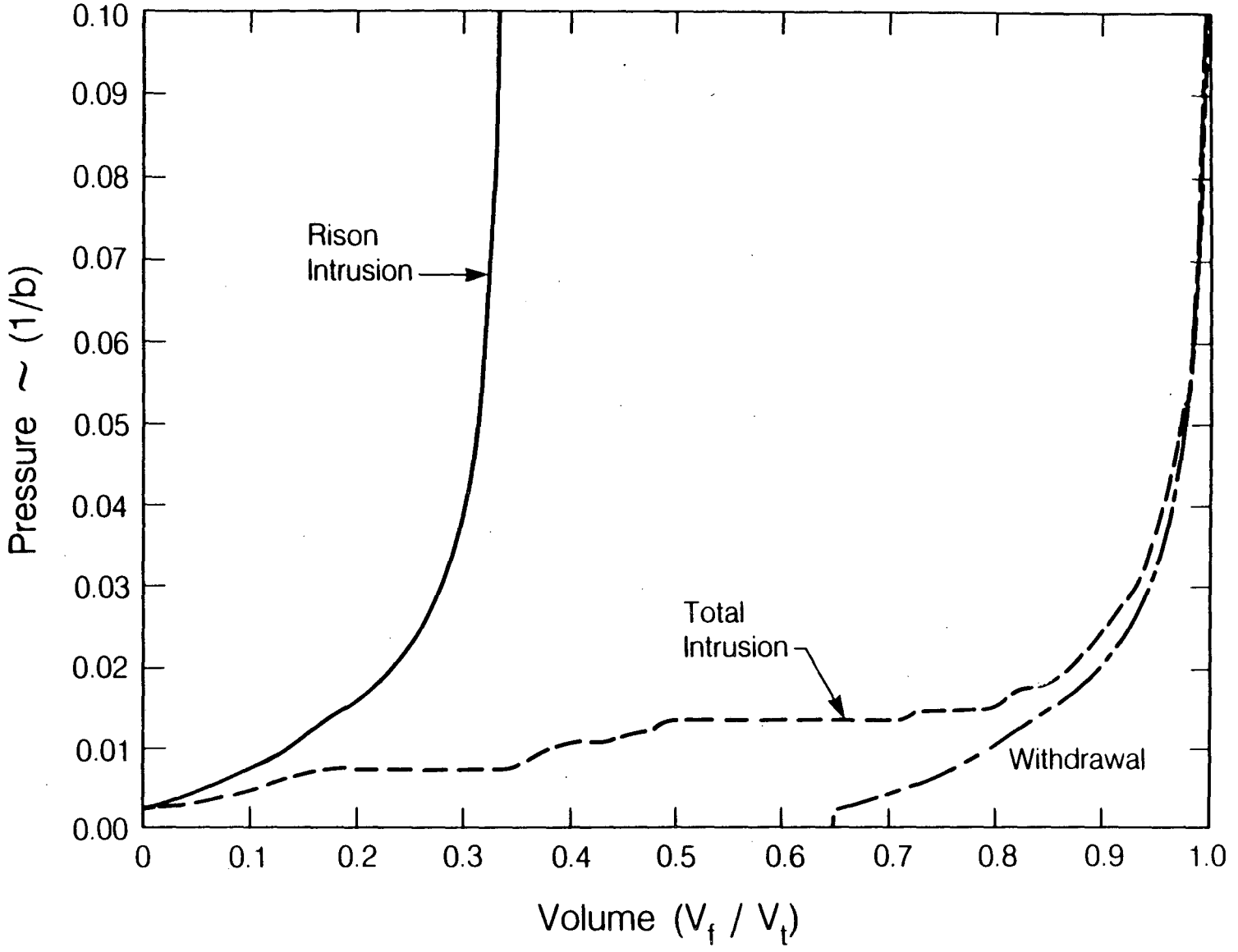

XBL 886-10265

Figure 4. Simulated capillary pressure curves for pressure-controlled and rate-controlled porosimetry measurements.

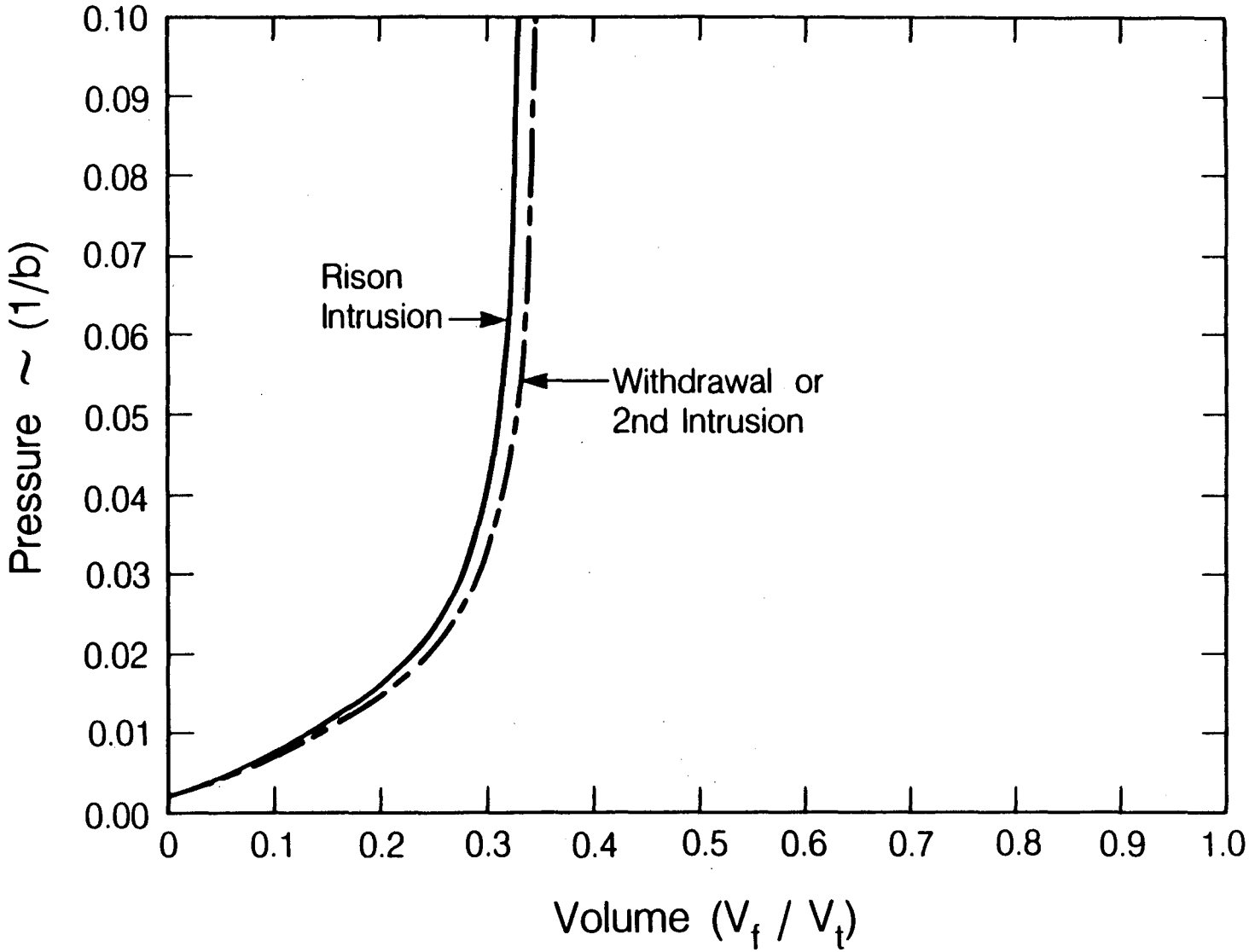

XBL 886-10264

Figure 5. Simulated capillary pressure curves for second intrusion in pressure-controlled measurements.

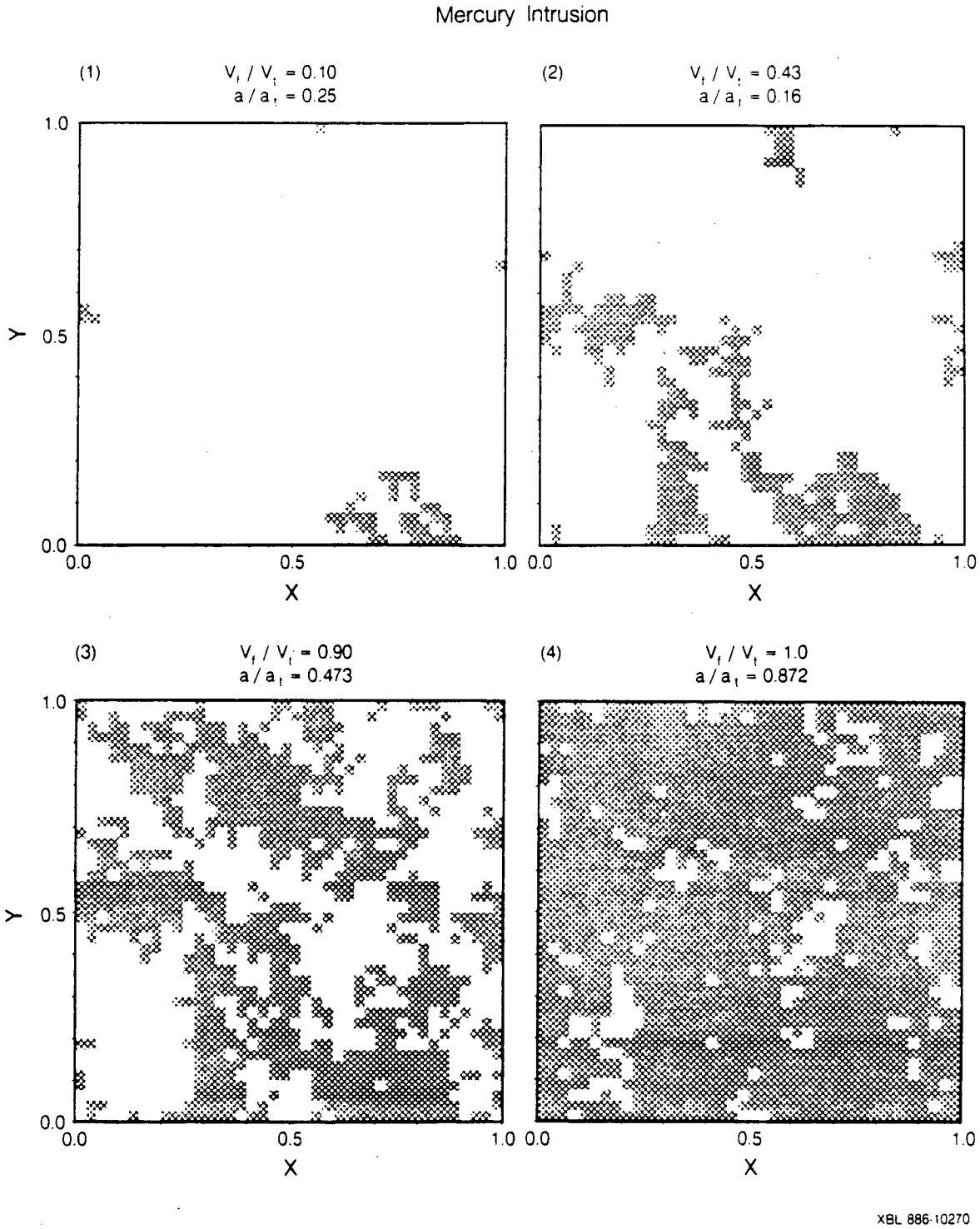

Figure 6. Time sequence of mercury intrusion into the fracture with aperture variation of Figure 2a.

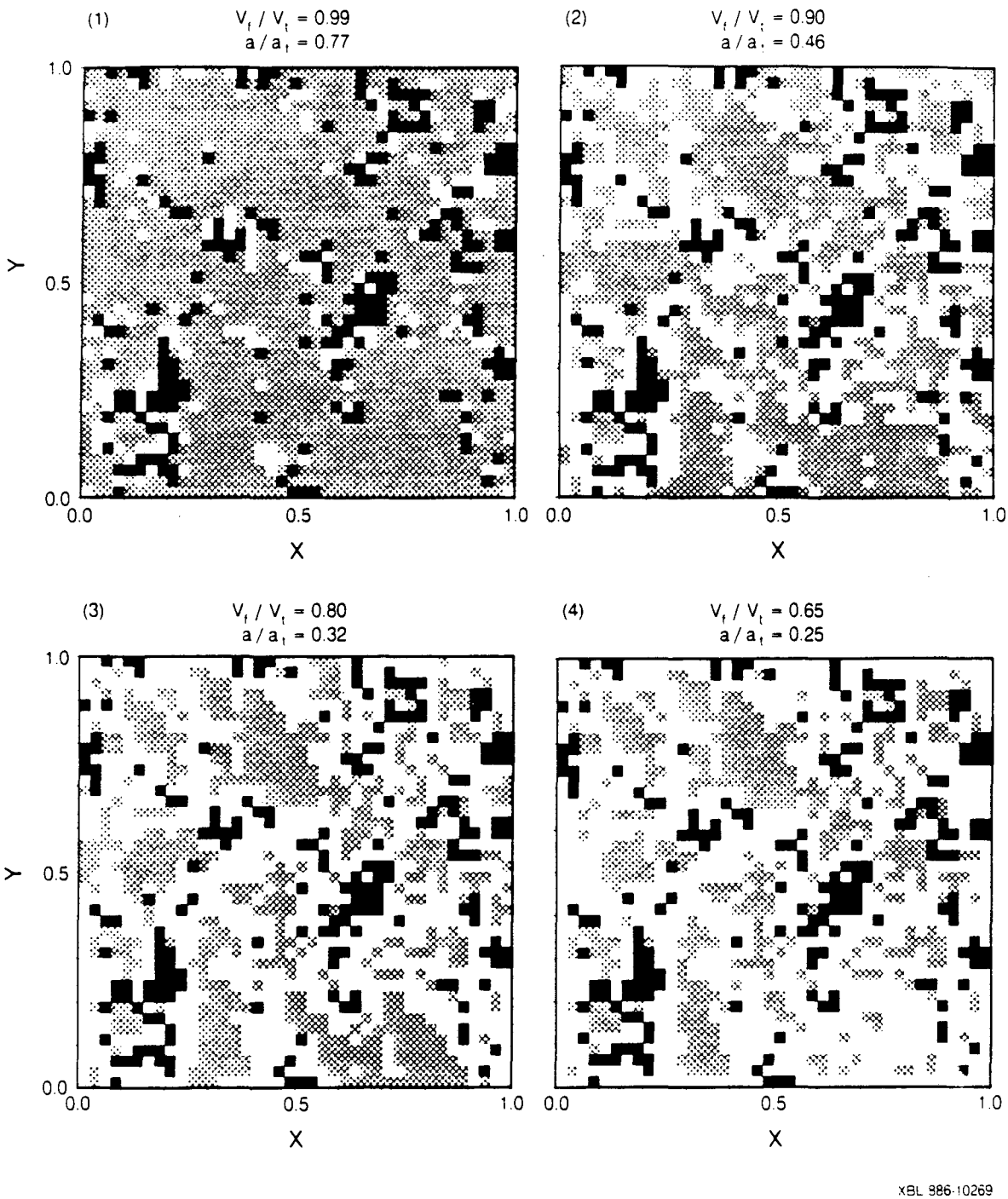

Figure 7. Time sequence of mercury withdrawal from the fracture with aperture variation of Figure 2a.

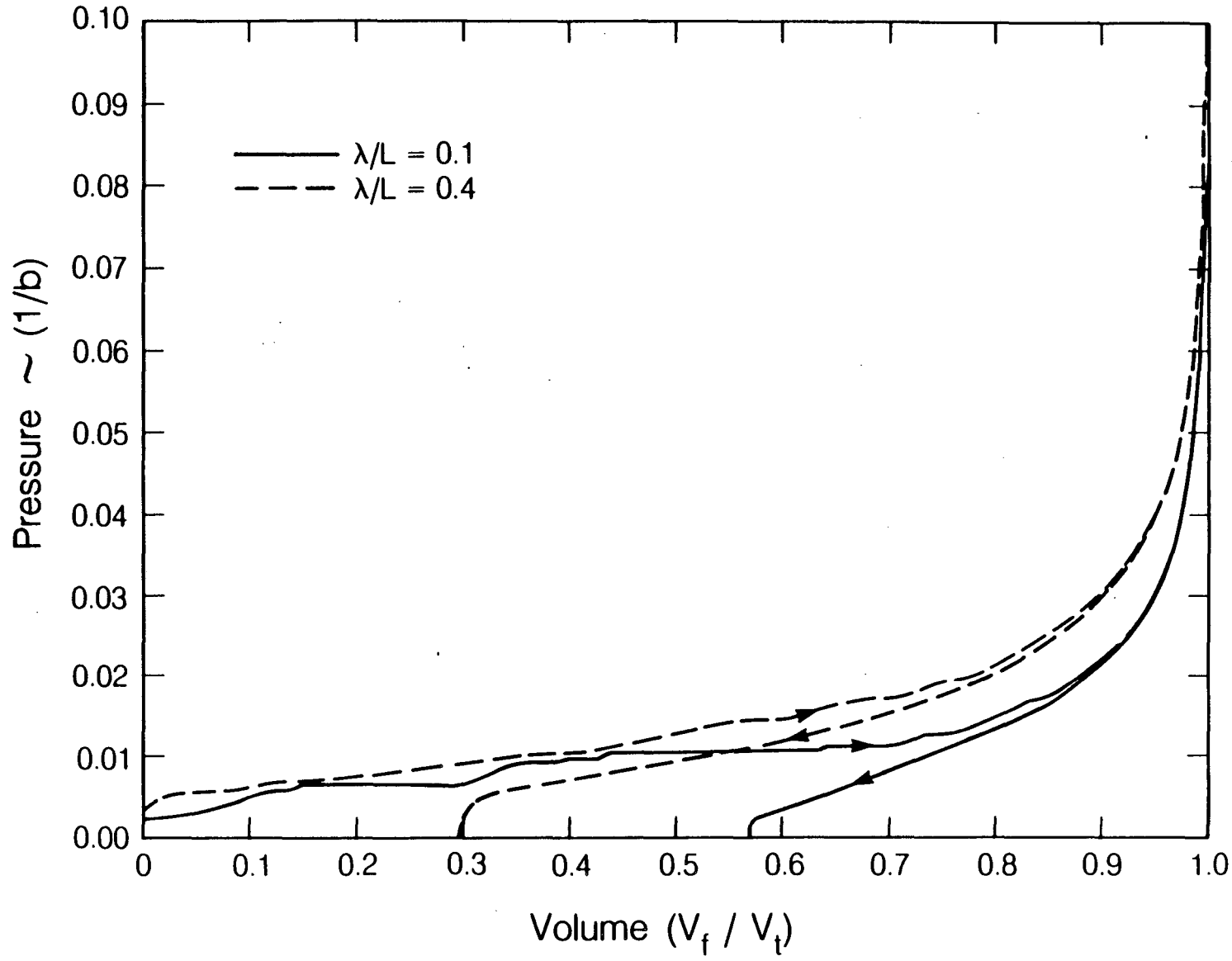

XBL 886-10263

Figure 8. Intrusion and withdrawal capillary pressure curves for the two fractures in Figure 2.

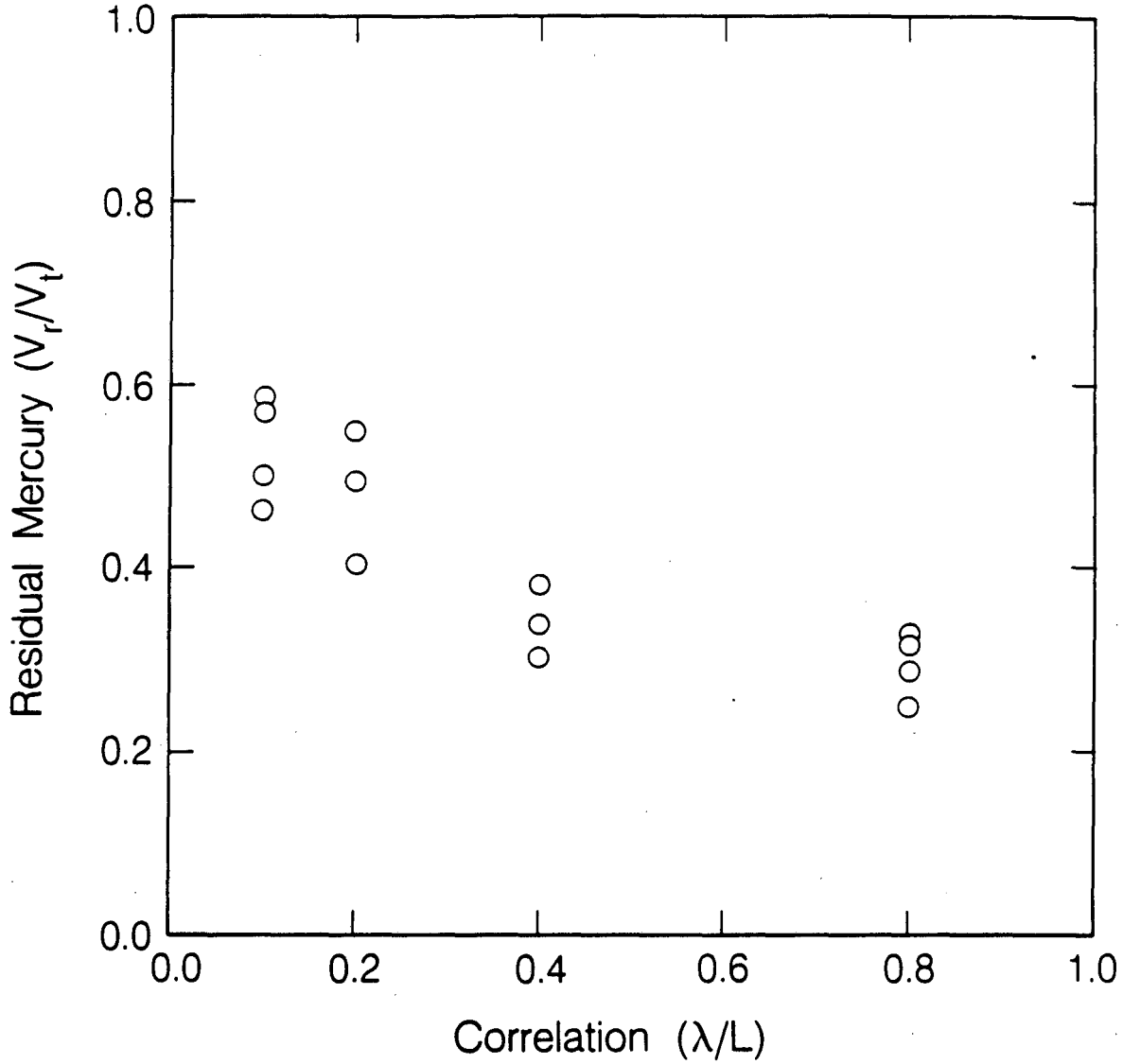

Figure 9. Fraction of trapped residual mercury as a function of spatial correlation length of the aperture spatial variation.

LAWRENCE BERKELEY LABORATORY
TECHNICAL INFORMATION DEPARTMENT
UNIVERSITY OF CALIFORNIA
BERKELEY, CALIFORNIA 94720